ELSEVIER

Materials Science and Engineering B 126 (2006) 230–235

MATERIALS SCIENCE & ENGINEERING B

www.elsevier.com/locate/mseb

Alloying, co-doping, and annealing effects on the magnetic and optical properties of MOCVD-grown $Ga_{1-x}Mn_xN$

Matthew H. Kane [a,b], Martin Strassburg [a,d], Ali Asghar [a], William E. Fenwick [a], Jayantha Senawiratne [c], Qing Song [d], Christopher J. Summers [b], Z. John Zhang [d], Nikolaus Dietz [c], Ian T. Ferguson [a,*]

[a] *Georgia Institute of Technology, School of Electrical and Computer Engineering, Atlanta, GA 30332, USA*
[b] *Georgia Institute of Technology, School of Materials Science and Engineering, Atlanta, GA 30332, USA*
[c] *Georgia State University, Department of Physics and Astronomy, Atlanta, GA 30303, USA*
[d] *Georgia Institute of Technology, School of Chemistry and Biochemistry, Atlanta, GA 30332, USA*

Abstract

Recent theoretical work for $Ga_{1-x}Mn_xN$ predicts ferromagnetism in this materials system with Curie temperatures above room temperature. Ferromagnetic behavior observed in $Ga_{1-x}Mn_xN$ is still controversial, as there are conflicting experimental reports owing to the disparity in crystalline quality and phase purity of $Ga_{1-x}Mn_xN$ produced by different methods. In this work, metal–organic chemical vapor deposition (MOCVD) has been used to grow high-quality epitaxial films of $Ga_{1-x}Mn_xN$ of varying thickness and manganese doping levels using Cp_2Mn as the Mn source. Crystalline quality and phase purity were determined by high-resolution X-ray diffraction, indicating that no macroscopic second phases are formed. Atomic force microscopy revealed MOCVD-like step flow growth patterns and a mean surface roughness of 0.378 nm in optimally grown films, which is close to that from the as-grown template layer of 0.330 nm. No change in the growth mechanism and morphology with Mn incorporation is observed. A uniform Mn concentration in the epitaxial layers is confirmed by secondary ion mass spectroscopy. SQUID measurements showed an apparent room temperature ferromagnetic hysteresis with saturation magnetizations of over 2 μ_B/Mn at $x = 0.008$, which decreases with increasing Mn incorporation. Upon high-temperature annealing, numerous changes are observed in these properties, including an increase in surface roughness due to surface decomposition and a large decrease in the magnetic signature. A similar decrease in the magnetic signature is observed upon co-doping with the shallow donor silicon during the growth process. These results demonstrate the critical importance of controlling the Fermi level relative to the $Mn^{2+/3+}$ acceptor level in $Ga_{1-x}Mn_xN$ in order to achieve strong ferromagnetism.

Keywords: Doping; Metalorganic chemical vapor deposition; Magnetic materials; Semiconducting compounds

1. Introduction

Recent predictions of room temperature ferromagnetism in novel semiconductor materials have spawned a great interest in semiconductor-based spintronics [1]. In pursuit of this goal, dilute magnetic semiconductors (DMS), which consist of semiconductors doped with rare earth or transition metals to provide magnetic functionality, have been studied for use in spintronic devices because of their unique electrical and magnetic properties [1–3]. These properties allow control of electron spin as well as charge flow, making the materials ideal for spintronic applications; their similarity to existing semiconductors shows promise for seamless integration with existing semiconductor technology.

The most widely studied of these III–V DMS compounds is $Ga_{1-x}Mn_xAs$ [4], which exhibits a close coupling between the carrier concentration and Curie temperature [5], and has been demonstrated to be effective at providing a spin injection layer in optically based devices [6]. Unfortunately, in this materials system the Curie temperature is limited to well less than 200 K, which renders the system unsuitable for practical purposes. One methodology for enhancing the Curie temperature is to employ smaller bond length materials with lower spin-orbit couplings, as would be found in transition metal-doped nitrides. $Ga_{1-x}Mn_xN$ films that exhibit ferromagnetism above room temperature are now possible due to recent developments in the growth of DMS. Room temperature ferromagnetism has been observed in $Ga_{1-x}Mn_xN$ films grown by metal organic

* Corresponding author.
E-mail address: ianf@ece.gatech.edu (I.T. Ferguson).

0921-5107/$ – see front matter © 2005 Elsevier B.V. All rights reserved.
doi:10.1016/j.mseb.2005.09.056

chemical vapor deposition (MOCVD) [7], molecular beam epitaxy (MBE) [8], Mn-implanted GaN epilayers [9], and post growth diffusion of Mn into GaN [10]. Ferromagnetic behavior is still highly controversial, as there are several competing theoretical approaches to explain the origin of room temperature ferromagnetism in group III nitrides [1,11–13]. The thermodynamic tendency towards forming ferromagnetic second phases and/or nanoclusters increases in the complexity of this field. It is often unclear whether the observed ferromagnetism is due to substitutional Mn ions in the semiconductor lattice, unwanted precipitates, or a combination of both.

All of the current models for explaining ferromagnetism show a gradual increase in the Curie temperature with increasing Mn doping level. Dietl et al. [1] proposed the original theory that predicted high T_C in the wide bandgap materials, suggesting that ferromagnetic ordering in Mn-doped dilute magnetic semiconductors is mediated by the charge carriers in the material. This carrier-mediated mean field p–d exchange theory predicts a Curie temperature that is dependent on the localized spin concentration as well as carrier concentration. Room temperature ferromagnetism is predicted at Mn concentrations above 5%. Using first principles, it has been shown that the band structure of $Ga_{1-x}Mn_xN$ exhibits a strong splitting in the density of states function within a midgap impurity band [14–17]. Using a mean field approximation and Zener's double exchange model, the Curie temperature has been predicted to be above room temperature at concentrations of 1%, however, more recent Monte Carlo simulations suggest that this prediction does not hold and that due to the highly localized nature of the Mn wavefunctions in the deep acceptor level [18], the Curie temperature should be less than 100 K. An alternate method for impurity band formation suggests that formation of magnetic polarons may promote the formation of a spin split impurity band [11], though this should occur after some sort of percolation limit. Thus, the magnetic behavior strongly depends on the amount of manganese site disorder. Developing a comprehensive model for the differing behavior in this system will require an analysis of how the processing technique affects the Mn atomic arrangement. It is interesting to note that all of the reported Curie temperatures for $Ga_{1-x}Mn_xN$ fall within the limits of the metallic perovskite phase $Mn_{4-x}Ga_xN_{1-y}$, which exhibits Curie temperatures from 270 to 743 K with increasing manganese concentration due to Ga–Mn site disorder. This materials system has been shown to be one of the key decomposition products under annealing or non-optimal growth of these compounds [19,20], and this phase does have arrangements where it is commensurate with the wurtzite lattice [10].

2. Experimental

$Ga_{1-x}Mn_xN$ films with Mn concentration up to ∼2% were grown in an MOCVD D-125 rotating disk reactor with a short jar configuration and specially designed reactant injection system which has been modified with dual injector blocks to minimize prereactions of the gallium and manganese precursors in the transport phase. Mn concentration in the film was varied up to ∼2% by controlling the molar flow ratios of the cursors. All films were grown near standard GaN growth temperatures on 2″ sapphire (0 0 0 1) substrates. Initially, GaN buffer layer templates with a thickness of 1–2 μm were grown, followed by $Ga_{1-x}Mn_xN$ with thicknesses ranging from 300 to 1000 nm. Ammonia, trimethyl gallium (TMG), trimethyl aluminum (TMA) and bis-cyclopentadienyl manganese (Cp_2Mn), bis-cyclopentadienyl magnesium (Cp_2Mg) and silane (SiH_4) were used as the nitrogen, gallium, aluminum, manganese, p-, and n-dopant sources, respectively, for $Ga_{1-x}Mn_xN$. A Renishaw micro-Raman system with a 488 nm excitation source was used for Raman measurements. High-resolution X-ray diffraction was performed with a Philips X′Pert Pro diffractometer. Secondary ion mass spectroscopy (SIMS) depth profiles were performed on the samples using an Atomika Instruments Ionmicroprobe A-DIDA 3000. Atomic force microscopy (AFM) was performed using a PSIA XE-100. Magnetic properties were analyzed using a Quantum Design MPMS 5S SQUID magnetometer at temperatures from 5 to 300 K; additional room temperature magnetization measurements were performed with a Lakeshore 7404 Vibrating Sample magnetometer. Transmission measurements were performed using the red and infrared spectrum of a halogen lamp with the transmitted light was detected by a photomultiplier attached to a 0.24 m monochromator with a spectral resolution of better than 6 nm. Some samples were subsequently annealed face-down on GaN templates in flowing nitrogen ambient at temperatures ranging from 700 to 900 °C.

3. Results

The as-grown films $Ga_{1-x}Mn_xN$ were specular and exhibited increasing reddish color with increasing thickness and Mn incorporation. Varying the temperature outside the optimal growth band resulted in the appearance of hexagonal GaN growth temperature defects which were visible via optical microscopy, or in the loss of film integrity as evidenced by in situ reflectometry. SIMS verified the uniform incorporation of manganese within the layers. In the X-ray diffraction scans, no second phases were observed in the as-grown samples as shown in Fig. 1. The position of the $Ga_{1-x}Mn_xN$ peaks did not shift relative to the GaN at low doping levels, indicating a lattice parameter similar to that of GaN. Renninger scans have recently been demonstrated as an effective tool for monitoring crystalline quality in Wurtzite layers [21]. A phi scan at the GaN(0 0 0 1) reflection in GaN and $Ga_{1-x}Mn_xN$ with no underlying GaN template is shown in Fig. 1. The two curves virtually superimpose, indicating little degradation in overall structural quality in the $Ga_{1-x}Mn_xN$. Linewidths for ω–2θ scans on the (0 0 0 2) and (10–12) reflections in samples doped at ∼1% Mn were 150 and 522 arc sec, compared with 179 and 518 arc sec for the underlying template layer. Upon annealing in non-reactive nitrogen atmospheres at temperatures as low as 700 °C, other phases appeared in the ω–2θ scans.

Additional information about the growth mechanism of $Ga_{1-x}Mn_xN$ and annealing effects is derived from studies of surface morphology using atomic force microscopy images to study the $Ga_{1-x}Mn_xN$ layers. Fig. 2 shows images of a typical as-grown layer and a layer annealed at 900 °C. The overall film

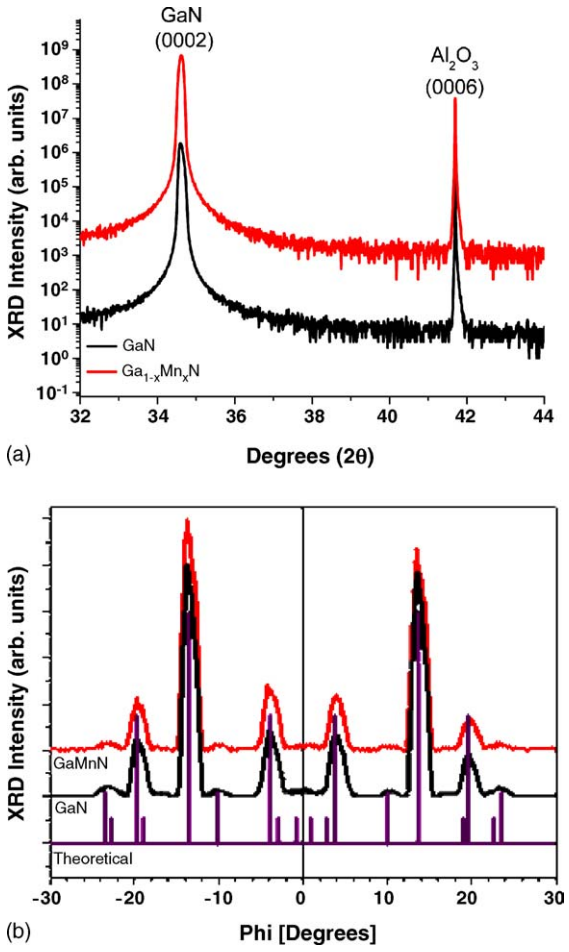

Fig. 1. (a) XRD scans of undoped (bottom) and Mn-doped GaN (top), exhibiting no observable change in lattice parameter, phase purity, or XRD linewidth. (b) Renninger scan of forbidden GaN(0 0 0 1) peak in undoped (bottom) and Mn-doped GaN (top), along with the predicted location of the XRD double reflection peaks.

quality is smooth as clear step flow growth patterns are seen in the as-grown MOCVD sample scans, which are typical of two-dimensional growth modes in GaN MOCVD. The root mean square (rms) values of the surface roughness are between 0.3 and 1.1 nm, depending on the underlying template layer. This mode does not change with the introduction of Mn into the growth process. There is little change in the morphology of the layer with low temperature annealing (700 °C). However, there is a significant difference in the AFM images with annealing at higher temperatures. The AFM image of the uncapped sample annealed at 900 °C shows clear areas of what is likely second phase precipitate on the surface. This suggests that the primary mechanism for the decay of the thermodynamically unstable $Ga_{1-x}Mn_xN$ compound is nitrogen desorption and phase rearrangement of the surface at the $Ga_{1-x}Mn_xN$-to-atmosphere interface in the absence of a reactive nitrogen environment that is present during MBE or MOCVD growth. This decomposition mechanism may also explain the enhanced thermal stability of $Ga_{1-x}Cr_xN$ films [22], which have a higher Cr pinning impurity band level, and thus less of a thermodynamic tendency for nitrogen vacancy formation [23] which would lead to structural degradation of the films.

SQUID magnetometry was performed to determine the overall magnetic behavior of the MOCVD-grown $Ga_{1-x}Mn_xN$ films. Ferromagnetic hysteresis was recorded in the as-grown $Ga_{1-x}Mn_xN$ films. No evidence of second phases or superparamagnetic clusters was observed in the magnetic property data. Fig. 3 shows representative magnetization behavior of these samples. The curves are shown at 300 K; in general, there is little deviation for these curves at 5 K, indicating that the hysteresis is likely due to a phase with a high Curie temperature ($T_C > 400$ K). The saturation magnetization of the as-grown $Ga_{1-x}Mn_xN$ samples with $x = 0.008$ is 1.16×10^4 A/M which, based on the expected doping levels associated with the precursor molar flows, corresponds to a magnetic moment of 2.4 μ_B/Mn. Vibrating sample magnetometry confirms a stronger moment with field parallel vice perpendicular to the plane of the film. As seen in Fig. 3, upon annealing at 800 °C (where traces of surface precipitation may be seen via AFM) the magnetization of the same sample drops precipitously. There is still some area remaining in the hysteresis loop observed in this sample, indicating either that the ferromagnetic phase is not completely lost or there may be a small contribution from local areas of the alloy that were unaffected by the anneal or that consist of ferromagnetic second phases. A similar behavior for the magnetism is seen in the MOCVD-grown samples co-doped with silicon, where prior to co-doping, a large magnetic moment per atom can be seen. The magnetic moment decreases with increasing Si doping concentration and is nearly destroyed upon a target doping concentration greater than 10^{19}/cm^3 Si.

The large decrease in the magnetization with co-doping and annealing suggests a common origin to the deterioration of the magnetic properties of $Ga_{1-x}Mn_xN$. Recall the impurity band models of ferromagnetism (double exchange or exchange split

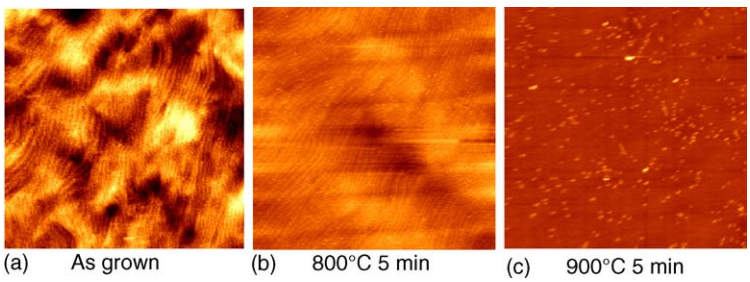

Fig. 2. Atomic force microscopy images of $Ga_{1-x}Mn_xN$ ($x = 0.015$) terminated MOCVD-grown $Ga_{1-x}Mn_xN$ samples, as-grown and annealed at 900 °C for 5 min. All scans are 10 μm × 10 μm. rms roughness values from left to right are 0.568, 0.594, and 0.771 nm.

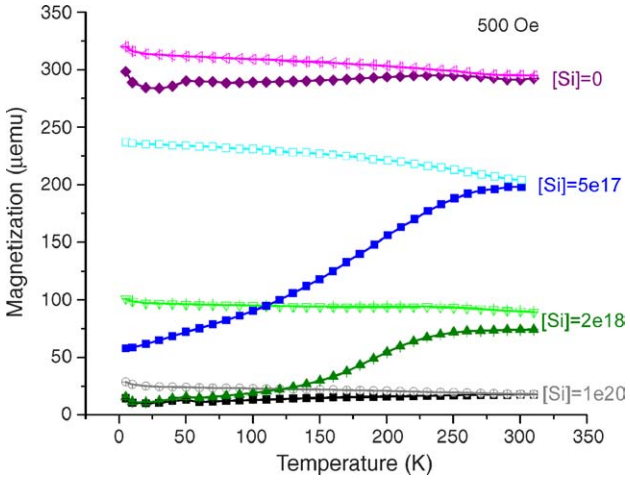

Fig. 3. Magnetization vs. applied field taken at room temperature with the applied field in the plane of the film for: (A) as-grown $Ga_{1-x}Mn_xN$ ($x = 0.008$), (B) as-grown $Ga_{1-x}Mn_xN$ ($x = 0.015$), (C) following 800 °C anneal, (D) co-doping with high levels of silicon (∼1e20). Note the decreased magnetic signature with annealing or silicon co-doping.

polaron models) in the DMS described above. In order to be able to support ferromagnetism, the Fermi level of the system must be in the spin split DOS Mn-impurity band, which is essentially midgap. The Fermi level must lie below the $Mn^{2+/3+}$ acceptor level so that the T_2 band is only partially filled and can support hopping and double exchange-like mechanism that stabilizes the ferromagnetism. Increasing the Fermi level by introducing donor states through either Si-codoping or annealing induced nitrogen vacancies above this level results in trapping of donor electrons, which fill the T_2 band. A conversion from the Mn^{3+} (d^4) to the Mn^{2+} (d^5) configuration ensues, thus eliminating the hopping pathway necessary for ferromagnetic ordering.

In order to reveal the charge state of the incorporated Mn ions incorporated in GaN, both transmission and emission studies were performed. The incorporation of Mn into GaN layers during MOCVD growth leads to a broad absorption band, a spectrally diffuse line around 1.5 eV, as shown in Fig. 4. These transitions have previously been observed in MBE-grown and implanted GaMnN epilayers [24,25]. The relatively large FWHM of ∼150 meV for this absorption band was observed, as

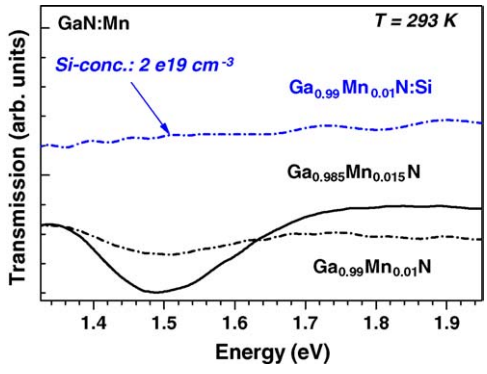

Fig. 4. Transmission spectra of $Ga_{1-x}Mn_xN$ with varying Mn concentrations. In addition, a transmission spectrum of a co-doped $Ga_{1-x}Mn_xN$:Si sample is shown. The spectrum of the Si co-doped sample is vertically shifted for clarity.

well as an increase of its FWHM and its intensity with increasing Mn concentration. Mn^{3+} transitions from the E state to the partially filled T_2 levels of the ^5D state are assigned to the observed absorption band; the broadening of these states is due to the high Mn concentration [17]. In comparison, no such absorption peak was observed in GaMnN epilayers that, by co-doping with Si during growth, had been prepared to exhibit n-type behavior. The absence of the absorption band around 1.5 eV in the $Ga_{1-x}Mn_xN$ layer co-doped with silicon indicates sensitivity of the E to T_2 transitions to the position of the Fermi level. The Fermi level is shifted towards the conduction band because electrons are present at deep defects. No other absorption features were detected further in the infrared spectral range (down to 0.5 eV). This suggests that the location of the Fermi level in the investigated samples in the broad absorption band is around 1.8 eV above the top of the valence band, and even closer to the conduction band than for the Si co-doped sample. Electrical property measurements on the $Ga_{1-x}Mn_xN$ films are highly dependent on the underlying layer; for films grown with a $Ga_{1-x}Mn_xN$ vice GaN buffer layer, the samples are too resistive to measure by standard means, consistent with the assignment of a deep trap state. However, an unambiguous proof that this Mn-induced band causes RT FM via a double exchange-like interaction is still needed and will be addressed by spin-sensitive spectroscopic techniques.

A more detailed study of the local and long-range lattice properties was performed by Raman spectroscopy. Fig. 5 shows Raman spectra for the as-grown $Ga_{1-x}Mn_xN$ samples and the ion-implanted samples. The spectra are dominated by the GaN E_2 (high) mode at 569 cm^{-1}. This peak is shifted by 2 cm^{-1} from the relaxed value of 567 cm^{-1} due to tensile strain as a result of the growth on sapphire substrates. Other Raman modes detected at 735, 560, and 533 cm^{-1} (A_1(LO), E_2(TO) and A_1(TO), respectively) were assigned to the GaN host lattice. The presence of a strong A_1(LO) mode confirms the absence of free carriers within this system due to the large binding energy of the Mn acceptors. No correlation of these modes to the Mn concentration was observed by Raman studies. The Raman modes around 160, 300, and 669 cm^{-1} appeared to be more sensitive to Mn incorporation. The intensities of these modes increased with Mn concentration, but no significant shift in their mode energies was observed. Similar behavior was detected for a shoulder near 610 cm^{-1}, though low intensity prevented deeper insight into the nature of this band. The two low-energy Mn disorder-activated modes result from defect densities that cause a loss of wave vector conservation in the scattering process [26,27]. Comparison of the measured Raman spectra with phonon-dispersion curves for hexagonal GaN shows that the broad peak at 300 cm^{-1} is a disorder-activated mode attributed to the highest acoustic phonon branch [26,27]. It should be noted that in this study the intensity of these modes is significantly lower (normalized to the E_2 (high) mode) compared to other reports, suggesting that MOCVD growth results in the generation of less lattice disorder due to Mn incorporation [26–29].

The features near 669 cm^{-1} were studied in more detail, as shown in Fig. 5. An asymmetric broadening of this mode revealed a substructure that can be fitted with an additional mode

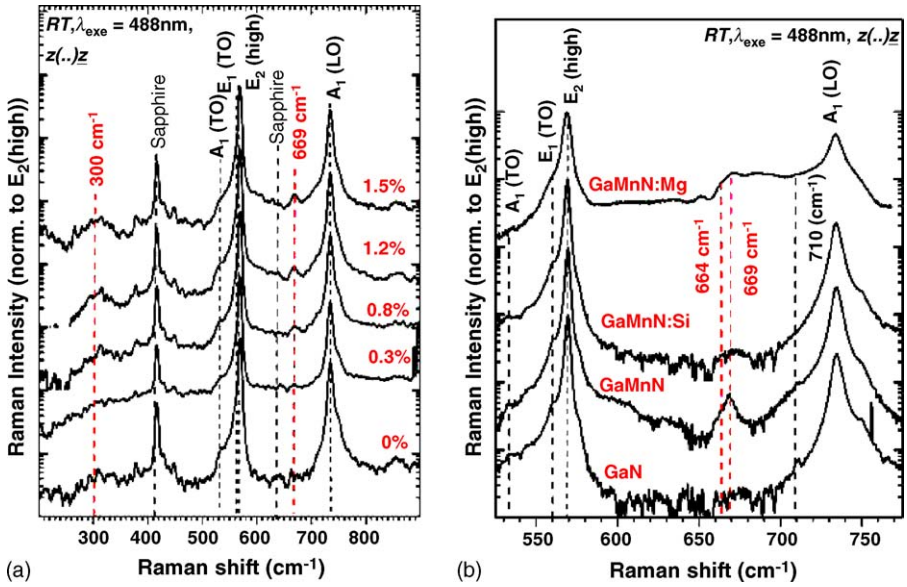

Fig. 5. Raman spectra of $Ga_{1-x}Mn_xN$ with increasing Mn concentrations. A disorder band at 300 cm^{-1} and vacancy-related band at 669 cm^{-1} are visible. (b) Si co-doping decreases the intensity of the 669 cm^{-1} mode.

at 664 cm^{-1}. These modes have previously been attributed to local vibrational modes (LVM) due to vacancies through the use of polarization dependent Raman studies [26–29]. This mode is assigned to nitrogen vacancies according to the growth conditions, which self-compensate the Mn acceptor-type defects. Photoluminescence measurements show broad emission band ranging from 2.7 to 3.1 eV in the as-grown samples which also suggests compensation in the MOCVD-grown $Ga_{1-x}Mn_xN$ epilayers. Si co-doping providing shallow donor states in GaN can be applied to suppress the intensity of the formation of nitrogen vacancies, as shown in Fig. 5. Vacancy formation is also suggested by the infrared reflection data which shows a weakening of the GaN lattice with heavy Mn incorporation [30].

The intensities of the modes at 664, 669, and 710 cm^{-1} were found to be strongly dependent on Mn concentration (inset of Fig. 5). For comparison, the intensity of the A_1(LO) mode does not change with Mn concentration. While the 710 cm^{-1} mode scales even more with the Mn concentration, but this mode is due to mixing of Raman modes from different points of the Brillioun zone and is outside the scope of this study.

4. Conclusions

$Ga_{1-x}Mn_xN$ has been produced with varying Mn doping levels by MOCVD. The films exhibited no secondary phases under optimal growth conditions, though some Mn-induced disorder was seen in the films with increasing doping levels via Raman spectroscopy. Annealing of the films caused a loss of surface integrity and a decrease in magnetization. The latter also occurred upon co-doping with Si. Optical studies revealed a Mn-related photoabsorption band which correlated with stronger ferromagnetism in the $Ga_{1-x}Mn_xN$ films.

References

[1] T. Dietl, H. Ohno, F. Matsukura, J. Cibert, D. Ferrand, Science 287 (2000) 1019.
[2] S.J. Pearton, C.R. Abernathy, M.E. Overberg, G.T. Thaler, D.P. Morton, J. Appl. Phys. 93 (2003) 1.
[3] T. Dietl, Phys. Status Solidi B 240 (2003) 433.
[4] H. Ohno, A. Shen, F. Matsukura, A. Oiwa, A. Endo, S. Katsumoto, Y. Iye, Appl. Phys. Lett. 69 (1996) 363.
[5] K.C. Ku, S.J. Potashnik, R.F. Wang, S.H. Chun, P. Schiffer, N. Samarth, M.J. Seong, A. Mascarenhas, E. Johnston-Halperin, R.C. Myers, A.C. Gossard, D.D. Awschalom, Appl. Phys. Lett. 82 (2003) 2302.
[6] Y. Ohno, D.K. Young, B. Beschoten, F. Matsukura, H. Ohno, D.D. Awschalom, Nature 402 (1999) 790.
[7] M.H. Kane, A. Asghar, A.M. Payne, C.R. Vestal, M. Strassburg, J. Senawiratne, Z.J. Zhang, N. Dietz, C.R. Summers, I.T. Ferguson, Semicond. Sci. Technol. 20 (2005) L5.
[8] M.E. Overberg, C.R. Abernathy, S.J. Pearton, N.A. Theodoropoulou, K.T. McCarthy, A.F. Hebard, Appl. Phys. Lett. 79 (2001) 1312.
[9] Y. Shon, Y.H. Kwon, D.Y. Kim, D. Fu, T.W. Kang, Jpn. J. Appl. Phys. 40 (2001) 5304.
[10] M.L. Reed, N.A. El-Masry, H.H. Stadelmaier, M.K. Ritums, M.J. Reed, C.A. Parker, J.C. Roberts, S.M. Bedair, Appl. Phys. Lett. 79 (2001) 3473.
[11] M. Berciu, R.N. Bhatt, Phys. Rev. Lett. 87 (2001) 107203.
[12] K. Sato, H. Katayama-Yoshida, Semicond. Sci. Technol. 17 (2002) 367.
[13] J.M.D. Coey, M. Venkatesan, C.B. Fitzgerald, Nat. Mat. 4 (2005) 173.
[14] L. Kronik, M. Jain, J.R. Chelikowsky, Phys. Rev. B 66 (2002) 041203.
[15] K. Sato, H. Katayama-Yoshida, Phys. Status Solidi B 229 (2002) 673.
[16] H. Katayama-Yoshida, K. Sato, Physica B 327 (2003) 337.
[17] K. Sato, P.H. Dederichs, H. Katayama-Yoshida, J. Kudrnovsky, Physica B 340–342 (2003) 863.
[18] P. Mahadevan, A. Zunger, Appl. Phys. Lett. 85 (2004) 2860.
[19] S. Kuroda, E. Bellet-Amalric, X. Biquard, J. Cibert, R. Giraud, S. Marcet, H. Mariette, Phys. Status Solidi B 240 (2003) 443.
[20] M.H. Kane, A. Asghar, M. Strassburg, Q. Song, A.M. Payne, C.J. Summers, Z.J. Zhang, N. Dietz, I.T. Ferguson, MRS Proc. 831 (2005) E9.4.1.
[21] J. Blasing, A. Krost, Phys. Status Solidi A 201 (2004) R17.
[22] G. Thaler, R.M. Frazier, C.R. Abernathy, S.J. Pearton, Appl. Phys. Lett. 86 (2005) 131901.

[23] A. Zunger, Appl. Phys. Lett. 83 (2003) 57.
[24] T. Graf, M. Gjukic, M.S. Brandt, M. Stutzmann, O. Ambacher, Appl. Phys. Lett. 81 (2002) 5159.
[25] O. Gelhausen, E. Malguth, M.R. Phillips, E.M. Goldys, M. Strassburg, A. Hoffmann, T. Graf, M. Gjukic, M. Stutzmann, Appl. Phys. Lett. 84 (2004) 4514.
[26] W. Limmer, W. Ritter, R. Sauer, B. Mensching, C. Liu, R. Rauschenbach, Appl. Phys. Lett. 72 (1998) 2589.
[27] M. Zajac, R. Doradzinski, J. Gosk, J. Szczytko, M. Lefeld-Sosnowska, M. Kaminska, A. Twardowski, M. Palczewska, E. Grzanka, W. Gebicki, Appl. Phys. Lett. 78 (2001) 1276.
[28] W. Gebicki, J. Strzeszewski, G. Kamler, T. Szyszko, S. Podsiadlo, Appl. Phys. Lett. 76 (2000) 3870.
[29] H. Harima, J. Phys. Condens. Matter 16 (2004) S5653.
[30] Z.G. Hu, M. Strassburg, N. Dietz, A.G.U. Perera, M.H. Kane, A. Asghar, I.T. Ferguson, Appl. Phys. Lett., submitted for publication.